Journal of Non-Crystalline Solids 386 (2014) 8–13

Contents lists available at ScienceDirect

Journal of Non-Crystalline Solids

journal homepage: www.elsevier.com/ locate/ jnoncrysol

Natural physical aging in glassy As–Se: A comparative study of chaotic behavior with enhanced results analysis

A.S. Hacinliyan [a,b,c,*], Y. Skarlatos [b,c], I. Kusbeyzi Aybar [d], O.O. Aybar [a,e], O. Shpotyuk [f,g], R. Golovchak [f,h], V. Balitska [f,i], A. Kozdras [j]

[a] Yeditepe University, Department of Information Systems and Technologies, Istanbul, Turkey
[b] Yeditepe University, Department of Physics, Istanbul, Turkey
[c] Bogazici University, Department of Physics, Istanbul, Turkey
[d] Yeditepe University, Department of Computer Education and Instructional Technology, Istanbul, Turkey
[e] Gebze Institute of Technology, Department of Mathematics, Gebze-Kocaeli, Turkey
[f] Lviv Scientific Research Institute of Materials of SRC "Carat", 202, Stryjska str., Lviv 79031, Ukraine
[g] Institute of Physics of Jan Dlugosz University, 13/15, al. Armii Krajowej, Czestochowa 42201, Poland
[h] Department of Physics and Astronomy, Austin Peay State University, Clarksville, TN 37044, USA
[i] Lviv State University of Vital Activity Safety, 35, Kleparivska str., Lviv 79007, Ukraine
[j] Institute of Physics, Mathematics and Chemistry of Opole Technical University, 75, Ozimska str., Opole 45370, Poland

ARTICLE INFO

Article history:
Received 25 September 2013
Received in revised form 8 November 2013
Available online xxxx

Keywords:
Chalcogenide glasses;
Irregular behavior;
Differential scanning calorimetry;
Natural physical aging

ABSTRACT

Theory of chaos is shown to be adequately applied to analyze kinetics of natural physical aging revealed in structural relaxation of Se-rich As–Se glasses below glass transition. Kinetics of enthalpy losses induced by prolonged storage in natural conditions is used to determine phase space reconstruction parameters. The observed chaotic behavior (involving chaos and fractal consideration such as detrended fluctuation analysis, attractor identification using phase space representation, delay coordinates, mutual information, and false nearest neighbors) reconstructed via TISEAN is treated within potential energy landscape as diversity of multiple transitions between different basins–metabasins towards more thermodynamically equilibrium state, minimizing the free energy of the system. Natural physical aging, facilitates further atomic shrinkage of the glass backbone.

1. Introduction

Although numerous models have been proposed for the photosensitivity of chalcogenide glasses (ChG), [1–4], little attention was paid to the kinetics in respect to native metastability proper to such kinds of glass-forming systems [5,6]. The effects of natural physical aging (NPhA) tending ChG towards more favorable thermodynamic states are able to significantly modify other phenomena in these disordered solids, including effects of externally-attained functionality [7–9].

Since ChG belong to a wide class of disordered solids, which are typical non-linear systems out of thermodynamic equilibrium, the theory of chaos in physical systems [10–13] can be used to analyze their time evolution. The *N*-particle system such as ChG can be imagined in terms of a hypothetical energy hypersurface of $3N + 1$ dimensions (energy/enthalpy landscape [13–15]), where the system's energy is determined by positions of all constituting particles and its dynamics is viewed as motion of "state point" described by coordinates of these particles along landscape surface [16,17]. Such landscape of complex glass system consists of many local minima of energy (inherent structures or attractors) and associated basins [13–17]. If the system with broken ergodicity can explore more than one (but finite) number of inherent structures at a particular temperature, they can be grouped together in larger metabasins [17,18]. In such a consideration, the NPhA can be viewed as a problem of transitions between different basins/metabasins towards more thermodynamically equilibrium state, minimizing the free energy of the system. In other words, all the trajectories of the particles should be attracted to a basin of attractions accessible under certain conditions after a sufficiently long time and finish there. This complicated scenario of hierarchically-arranged interbasin transitions results in stretched-exponential relaxation kinetics observed in a large number of polymer and glassy-like materials [5].

Although chaos is usually associated with long time predictability horizon of the system, it has been successfully tested in applications to transient current kinetics of typical polymer systems (polymethylmethacrylate and polyethylene glycol) [19,20]. Therefore, it should also be of help in elucidating the kinetics of below-T_g structural relaxation (PhA) in Se-rich As–Se glasses as typical representatives of ChG. This process is both a slow process and involves relaxation in a relatively disordered medium so that chaos theory is expected to be a useful tool. To our knowledge, use of chaos theory in such research is first, despite numerous papers on complicated kinetics of NPhA in

* Corresponding author at: Yeditepe University, Department of Information Systems and Technologies, Istanbul, Turkey. Tel.: +90 216 5780000/3024; fax: +90 216 5781672.
E-mail address: ahacinliyan@yeditepe.edu.tr (A.S. Hacinliyan).

0022-3093/$ – see front matter © 2013 Elsevier B.V. All rights reserved.
http://dx.doi.org/10.1016/j.jnoncrysol.2013.11.022

some ChG (see, for example [7,8] and references herein). Data on the kinetics of enthalpy losses induced by prolonged dark storage in natural conditions (NPhA) in glassy As–Se will be used to determine the phase space reconstruction parameters.

2. Experimental

The samples of glassy g-$As_{10}Se_{90}$, g-$As_{20}Se_{80}$ and g-$As_{30}Se_{70}$ were prepared by the conventional melt quenching route in evacuated quartz ampoules from a mixture of high purity precursors, as described elsewhere [21,22]. These typical ChG compositions were chosen owing to wide glass-forming regions of the above binary systems and previous data on the kinetics of PhA in a dark and under various external factors [21–23]. Glassy as opposed to metallic phase is distinguished by the high resistivity of the material (greater than 12 orders of magnitude as opposed to metals). Amorphous state and chemical composition of as-prepared ChG were controlled visually by a characteristic conch-like fracture, data of X-ray diffraction and X-ray photoelectron spectroscopy.

Bulk samples in the form of thick ~3 mm plates were sealed in hermetic plastic bags and stored in the dark at room temperature during more than two decades before calorimetric measurements. Before the experiments had started, all samples were rejuvenated by heating (~40 K) above corresponding onset values of glass transition temperature T_g to erase any thermal prehistory. The cooling rate during rejuvenation was the same as in the DSC measurements in a heating mode. Then, the aging procedure was arranged in a direct chronology so that samples were tested after defined storage steps from 1 day to 5 years.

The DSC measurements were performed on NETZSCH 404/3/F microcalorimeter pre-calibrated with a set of standard elements, the DSC traces being recorded in a dark at the ambient atmosphere with (5 K/min) heating rate. The same calibration procedure was repeated each time during routine kinetics measurements. Three independent DSC scans were performed in each case to confirm the reproducibility of the results. Finally, the raw DSC data were processed using the NETZSCH PC software package.

3. Results and discussion

3.1. Determination of real-time NPhA kinetics

Typical DSC curves recorded for investigated g-$As_{10}Se_{90}$ ChG after equal time intervals of natural dark storage are shown in Fig. 1. The NPhA behavior is revealed by DSC technique as the appearance of strong endothermic peak superimposed on the endothermic step of glass transition signal and its displacement towards higher temperatures [22–24]. The difference in the area under DSC signal of aged and rejuvenated ChG is directly proportional to the enthalpy losses ΔH [25]. As far as below-T_g structural relaxation is proper only to under-constrained networks [22–24], in further consideration we will focus only on NPhA expressed through corresponding $\Delta H(t)$ kinetics curves. It was established recently [26,27] that microstructural origin of NPhA in *Se*-based ChG relies on twisting of bridge chalcogen atoms between configurational structural states within double-well potentials. Three possible environments for Se atom were distinguished in *As–Se* ChG: *Se–Se–Se* fragments within Sen chains (number *n* of *Se* atoms in the chain is considered as a number of chalcogen atoms between As cations), *As–Se–Se* and *As–Se–As*. Each double-well potential associated with these fragments should have different energetic barrier and configurational parameters of state. Therefore, the activation energies for over-barrier transitions or tunneling of Se atoms between two neighboring states within double-well potential should be different, giving variety of possibilities to be externally activated. It is shown that twisting of Se atoms within double-well potential associated with Se–Se–Se fragments is responsible for the fast component of NPhA [25–27]. Such twisting leads to alignment of longer $Se_{n \geq 3}$ chains, their better space utilization followed by a fast shrinkage of surrounding network [25–27]. According to "chains crossing" model [21,22,28], the Se_n chains with $n \geq 3$ should fully disappear in g-As_xSe_{100-x} at $x \geq 25$. This leads to vanishing of relatively fast alignment-shrinkage in Se_n chains. On the other hand, the twisting of Se atoms within double-well potentials of *As–Se–Se* fragments and associated shrinkage of underconstrained glassy network are shown to have very slow kinetics (as testified by NPhA at room temperature) [25–31]. The kinetics of changes in partial area A under the endothermic peak in DSC experiments, enthalpy losses ΔH and fictive temperature T_f caused by dark storage of Se rich *g-As–Se* at room temperature exhibited a well-expressed step-wise character, showing some kinds of plateaus and steep regions [25]. A phenomenological description was sufficiently derived from the alignment-shrinkage mechanism of PhA, showing that experimental enthalpy relaxation kinetics is caused by a superposition of parallel/sequent alignment shrinkage processes with different relaxation times [25].

During NPhA the elementary relaxations of *Se* atoms within double-well potentials, associated with *Se–Se–Se* and *As–Se–Se* fragments, have a fluctuation nature. Randomly started at different sites in a sample bulk, they initiate further shrinkage of a glassy network due to contraction of free volume released during twisting (or alignment) of Se polymeric chains [34–36]. The effectiveness of these processes, however, depends significantly on the choice of chalcogen atom (*S* or *Se*). The structure of g-$As_{10}Se_{90}$ can be imagined within "chain crossing" model as composed of two types of *Se*-based units, *Se–Se–Se* and *As–Se–Se* with corresponding population of 2:1. So quick relaxation events originated from Se atoms twisting within *Se–Se–Se* chains dominates aging behavior in this ChG. As a result, the character step-wise kinetics caused by prolonged storage in natural conditions is proper to enthalpy losses in g-$As_{10}Se_{90}$ [25]. The process of NPhA is fully ended during two decades as it testified from fictive temperature T_f curve reaching room temperature [25]. The structure of g-$As_{20}Se_{80}$ is composed of *Se–Se–Se* and *As–Se–Se* units taken in a ratio 1:3. So twisting of Se atom surrounded by other Se and As atoms is dominated acting route, determining more prolonged time constants of structural relaxation in this ChG. The step-wise features are also visible in the NPhA kinetics of this glass, but they are less revealed in contrast to g-$As_{10}Se_{90}$ [25]. The process of NPhA does not reach saturation during two decades, since the corresponding T_f value remains above room temperature (340 K). In contrast, the structure of g-$As_{30}Se_{70}$ is significantly different being composed of As–Se–Se and As–Se–As units populated in a glassy matrix as 5:2 (estimation within "chain crossing" model). As a result, the quick relaxation processes are not character for this glass and corresponding T_f value remains far above room temperature (360 K) even after two decades of natural storage.

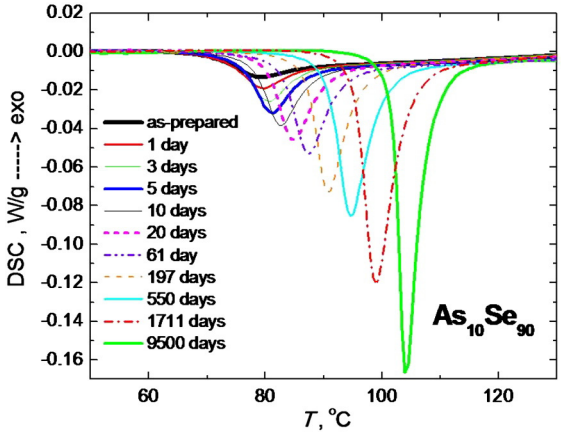

Fig. 1. DSC curves recorded at room temperature for g-$As_{10}Se_{90}$ after certain periods of NPhA.

3.2. Chaotic behavior observed in the kinetics of NPhA in g-As–Se

In this section, the analysis of chaotic behavior will be carried out using the standard time series methods, attractor reconstruction using phase space, embedding representation, delay coordinates, mutual information, false nearest neighbors (henceforth referred to as FNN) as described in the TISEAN [32,33] involving chaos and fractal analysis such as detrended fluctuation analysis (henceforth referred to as DFA). The details of the methods used have been reported elsewhere in [19,20]. We observe irregular transient enthalpy ΔH characteristics for studied ChG under NPhA as shown in Fig. 2. One way to understand this irregularity is to take increasing enthalpy losses H as a slowly varying parameter with the data split into equal time periods. After splitting, the delay times are analyzed using the delay-coordinate embedding theorem [32–36]. If the embedding is performed correctly, the theorem guarantees that the reconstructed dynamics of the system should be identical to true dynamics and dynamical invariants should also be identical. To work on time series at first we build up delay vectors $x(T), x(T+t), \ldots, x(T+(m-1)t)$. Here t and m represent delay time and embedding dimension, respectively. The reconstructed invariants (basically, its fractal dimension) of the attractor as found by this approach remain invariant with respect to the unknown, original system that generated the series. Fig. 2 demonstrates growing tendency in irregular enthalpy losses ΔH caused by NPhA in a sequence of g-$As_{30}Se_{70}$-g-$As_{20}Se_{80}$-g-$As_{10}Se_{90}$ (so with increase in an average covalent bonding). It is obvious that value of NPhA in g-$As_{30}Se_{70}$ is more than twice smaller as in g-$As_{10}Se_{90}$. At the same time, in Se-rich ChG, the pronounced "waves" appear at the beginning of NPhA, testifying in a favor of character step-wise kinetics caused by a superposition of parallel/sequent alignment shrinkage processes with different relaxation times [25].

3.3. Mutual information

In contrast to the linear dependence measured by the autocorrelation, mutual information $I(t)$, provides a measure of general dependence. Therefore $I(t)$ is expected to provide a better measure of the transition from small to large t with nonlinear systems. Mutual information answers the following question: given the observation of $S(T)$, at time T, how accurately can one predict $S(T+t)$ after a delay of t, so that successive delay coordinates are interpreted as relatively independent when the mutual information is small?

Let us assume that there exists two sets X and Y with x_i being the possible outcome of a measurement on X and y_j the possible outcome of a measurement on Y. If the measurement x_i is completely independent from y_j then

$$P_{XY}\left(x_i;y_j\right) = P(x_i)P\left(y_j\right). \tag{1}$$

The joint probability of observing x_i by a measurement of X and observing y_j by a measurement of Y, $P_{XY}(x_i;y_j)$, should be different from the product of the individual probabilities of measuring x and y out of the sets X and Y respectively, $P(x_i)$ and $P(y_j)$, if there is correlation between the two sets. The logarithm of that ratio in bits is therefore called the average mutual information of X and Y as below;

$$log_2 \frac{P_{XY}\left(x_i;y_j\right)}{P(x_i)P\left(y_j\right)}. \tag{2}$$

The weighted average of the average mutual information is given by the following formula:

$$I(X;Y) = -\sum_x \sum_y \left(P_{XY}\left(x_i;y_j\right)\right) log_2 \frac{P_{XY}\left(x_i;y_j\right)}{P(x_i)P\left(y_j\right)}. \tag{3}$$

To apply this formula to time series analysis, we assume that $S(n)$ as set X and $S(n+t)$ as set Y. Here we obtain the average mutual information as below

$$I(t) = -\sum_x \sum_y (P(s(n+t),s(n)) log_2 \left[\frac{P(s(n+t),s(n))}{P(s(n+t))P(s(n))}\right]. \tag{4}$$

It is natural to take time delay as a multiple of the sampling time of the time series. If time delay is taken too short, then components of the reconstructed vectors will be close to each other, causing the state space picture to appear on the diagonal line, therefore we will have loss of information about the real system. On the other hand, using a too long delay time will cause the correlations between components of reconstructed vectors to be lost and signals are mistakenly recognized as random [32,33,36,38]. We obtain the mutual information vs. time graph to decide the suitable delay time [36–38]. As t gets large, the behavior of the signal makes the measurements independent, hence the mutual information $I(t)$ goes to a minimum, preferably zero. In this graph of the mutual information, $I(X;Y)$, $I(t)$ starts off very high (given a measurement $S(t)$, we know as many bits as possible about $S(t+\sigma) \approx S(t)$, for σ zero or very small). As σ is increased, $I(\sigma)$ decreases, then usually rises again. It is suggested that the value of time delay where $I(\sigma)$ reaches its first minimum can be used for the state space reconstruction [33,36,38]. According to mutual information calculations given in Fig. 3, the delay time of NPhA in the tested glasses is quite similar being close to ~250 days despite glass composition. This specificity can be explained by preferential input of the same structural entities responsible for primary changes accompanied long-term NPhA in all glasses. In respect to microstructure study on NPhA origin in Se-rich binary *As–Se* glasses [22,25], these aging-related relaxation

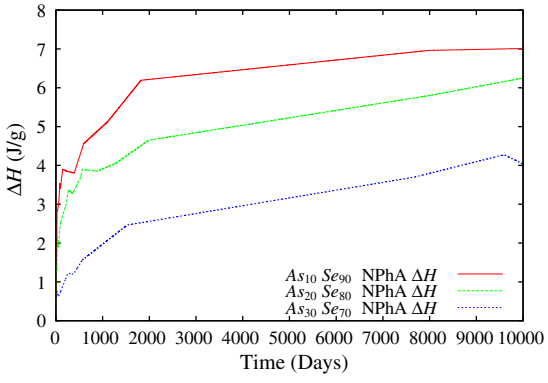

Fig. 2. DSC enthalpy vs. time $\Delta H - t$ graph for NPhA in g-$As_{10}Se_{90}$, g-$As_{20}Se_{80}$ and g-$As_{30}Se_{70}$.

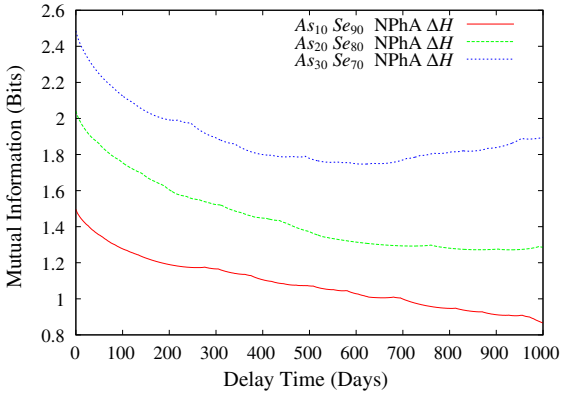

Fig. 3. Average mutual information vs. delay time graphs $I - t$ for NPhA in g-$As_{10}Se_{90}$, g-$As_{20}Se_{80}$ and g-$As_{30}Se_{70}$.

processes can be associated with twisting of inner Se atoms within heteropolar environment of character double-well potentials (mainly *As–Se–Se* fragments) [20,22,25,32,33,39,40].

3.4. Embedding dimension

Most of the systems in nature wander chaotically on a set of points called strange attractors. A related difficulty with attractor reconstruction involves the choice of the embedding dimension, *m*. After choosing an acceptable time delay we need a sufficiently large embedding dimension for the reconstructed phase space that avoids projecting the system onto a lower dimensional space. As mentioned before, the embedding theorem [33–35,37] tells us that if the box counting dimension of the attractor defined as *n*, an embedding dimension m that is greater *2n*, will absolutely allow unfolding the system in the reconstructed phase space. Normally, one has no a priori knowledge regarding the topological dimension, and it is unclear what a proper value of *m* would be.

One needs a criterion for the minimum embedding dimension, sufficient to unfold the attractor. At this point, the false nearest neighbors method is a useful tool to give an estimate for the embedding dimension. Suppose that a space reconstruction in dimension $m > m_0$ is carried out, where m_0 is the minimum dimension that unfolds the reconstructed attractor.

Beginning with the reconstructed data vectors in *m* dimensions with a proper time lag *t* and the time delay vector

$$y(k) = \left[s_{(k)}, s_{(k+t)}, \ldots\ldots, s_{(k+(m-1)t)}\right], \tag{5}$$

$y \in R^m$ in the embedded system with embedding dimension *m*, the nearest neighbors in phase space of the vector will be another time delay vector,

$$y_{NN}(k) = \left[s_{NN(k)}, s_{NN(k+t)}, \ldots, s_{NN(k+(m-1)t)}\right], \tag{6}$$

here $y(k)$ and $y_{NN}(k)$ are real embedded space neighbors so that they are presumed to arise from original neighbors of the dynamics of the system. As in the choice of time delays, if we chose an embedding dimension not large enough then the attractor will not unfold properly and because of the projection, false data points that are not neighbors will fall into each others neighborhood. Hence an increase in the embedding dimension will cause a decrease in the number of false neighbors, until we have taken a sufficiently large embedding dimension so that the decrease in the number of neighbors stabilizes.

Let R_d be real embedded space neighbors $y(k)$ and $y_{NN}(k)$ in m dimensions defined as

$$\|y(k) - y_{NN}(k)\|^2 = R_m^2, \tag{7}$$

$$\|y(k) - y_{NN}(k)\|^2 = \left[\left[s_{NN}(k) - s_{(k)}\right]^2 + \ldots + \left[s_{NN(k+(m-1)t)} - s_{(k+(m-1)t)}\right]^2\right]. \tag{8}$$

In $m + 1$ dimension $y(k)$ becomes $[s_{(k)}, s_{(k+t)}, \ldots\ldots, s_{(k+(m-1)t)}, s_{(k+(m-1+1)t)}]$, $y \in R^{m+1}$ and the distance between points embedded in m + 1 dimensions, $R_{m+1}(k)$ can be expressed in terms of $R_m(k)$ as

$$(R_{m+1}(k))^2 = (R_m(k))^2 + \left(s_{NN(k+(m)t)} - s_{(k+(m)t)}\right)^2. \tag{9}$$

From this result we can define a threshold value $R_T(k)$

$$\frac{\left[s_{NN(k+(m)t)} - s_{(k+(m)t)}\right]}{R_m(k)} > R_T(k) \tag{10}$$

so that points that satisfy this condition are assumed to be neighbors in *m* dimensions but not so in $m + 1$ dimensions. Such points are defined as false neighbors. For the Lorenz attractor, the minimal embedding dimension found by the method of false neighbors is 3. We can conclude from this result that if the embedding dimension exceeds three, there will be no false neighbors and the attractor will be unfolded in greater than or equal to three dimensions [34–38].

As in the choice of time delays [34–38], if we chose an embedding dimension not large enough, then the attractor will not unfold properly and because of the projection, false data points that are not neighbors will fall into each others' neighborhood. Hence an increase in the embedding dimension will cause a decrease in the number of false neighbors, until we have taken a sufficiently large embedding dimension so that decrease in the number of neighbors stabilizes. One counts the number of points that are neighbors in m dimensions, but not so in $m + 1$ dimensions. Such points are defined as false neighbors [34–38]. The false nearest neighbors approach uses the property of the attractor which guarantees that there are no two orbits that intersect each other. If the attractor is reconstructed in a space with small number of dimensions, then as a result of the projection, some orbits intersect each other. For the desired embedded dimension we should have a fraction of false neighbors that is close to zero within some tolerance. Turning this concept into an algorithm one would start with small values of *m* and calculate the number of false neighbors generated. One would then increase the number of dimensions one by one until the number of false neighbors is zero or nearly zero. This means that this number of dimensions is the best embedding for the system — the one with the least dimensions required to correctly represent the system.

By taking the delay time as given in Section 3.3, we analyzed the minimum embedding dimension to reconstruct the attractor by the false neighbors method as given in Fig. 4.

One may choose the smallest embedding dimension *m* that yields a convergent result. Due to the fact that chaotic systems are stochastic when embedded in a phase space that is very small to accommodate the true dynamics, we assume the embedding dimensions m as 4, 3 and 2 in that given order for NPhA for *g*-$As_{10}Se_{90}$, *g*-$As_{20}Se_{80}$ and *g*-$As_{30}Se_{70}$, respectively. It is important to note that this sequence in *m* values corresponds to smoothing tendency in NPhA kinetics, when multiple step-wise trends observed in Se-rich glasses (such as $g - As_{10}Se_{90}$) become smoother in glasses with less Se content (such as *g*-$As_{20}Se_{70}$ and *g*-$As_{30}Se_{70}$). It should be mentioned that the general structure of similar results for polymers studied previously [20,39] is the same as those for ChG samples.

3.5. Detrended fluctuation analysis

Confirmation of these characteristics mentioned in previous sections therefore requires a more detailed analysis of short and long range

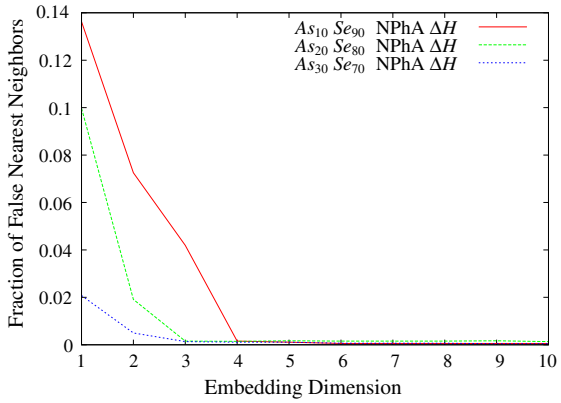

Fig. 4. Fraction of false nearest neighbors vs. embedding dimension graphs for NPhA in *g*-$As_{10}Se_{90}$, *g*-$As_{20}Se_{80}$ and *g*-$As_{30}Se_{70}$.

correlations in ChG. To investigate this in more details, we have applied the DFA method [20,39,40]. This is a scaling analysis method used to estimate long-range power-law correlation exponents. One integrates the time series of length N, then divides the result into boxes of equal length, n. The root-mean-square fluctuation of this integrated and detrended time series is calculated for all time scales (box sizes) to characterize the relationship between $F(n)$,

$$F(n) = \sqrt{\frac{1}{N}\sum_{k=1}^{N}\left(y(k) - y_n(k)\right)^2} \tag{11}$$

and the average fluctuation, as a function of box size, n [20,39,40]. A linear relationship on a log–log plot indicates the presence of power law scaling. Under such conditions, the fluctuations can be characterized by a scaling exponent, α, defined by the slope of the line related to $\log(F(n))$ and $\log(n)$.

The crossover in the scaling type of underlying correlation can be attributed to possible transition in the dynamical properties. In general, g-$As_{10}Se_{90}$, g-$As_{20}Se_{80}$ and g-$As_{30}Se_{70}$ subjected to NPhA have similar properties concerning more than one regime at the beginning and come closer to be on the same regime at the end as given in Fig. 5. As it follows from Fig. 5, the starting stages of NPhA in g-$As_{10}Se_{90}$ and g-$As_{20}Se_{80}$ have similar characteristics with slope of 1.57, changing this slope towards 1.90 with further stages, which is also the slope of NPhA for g-$As_{30}Se_{70}$.

In order to ascertain whether the linear interpolation is causing this uniformity, we have added 5% noise and used a stretched exponential extrapolation to construct the extrapolated data set [20]. The starting stages of NPhA in g-$As_{10}Se_{90}$ and g-$As_{20}Se_{80}$ have similar characteristics with slope of 0.56, changing the slope towards 1.90 which is also the slope of NPhA for g-$As_{30}Se_{70}$ as given in Fig. 6. Except for the increase in the embedding dimension and appearance of two regions (attributable to the noise introduced), similar conclusions follow. According to the detrended fluctuation analysis, slopes that are greater than 3/2 suggest Brownian motion therefore NPhA glasses show diffusion behavior like that in Brownian motion throughout the aging process.

4. Conclusion

Typical DSC traces of enthalpy losses ΔH caused by long-term NPhA of Se-rich As–Se glasses demonstrate an obvious evidence of chaotic behavior with character delay time in mutual information presentation close to 250 days despite glass composition and embedding dimensions decreasing in 4–3–2 sequence in a row of $As_{10}Se_{90}$–$As_{20}Se_{80}$–$As_{30}Se_{70}$ glasses (with increase in average covalent bonding). This sequence in m values corresponds to smoothing tendency in NPhA kinetics, when multiple step-wise trends observed in Se-rich g-$As_{10}Se_{90}$ become smoother in glasses with less *Se* content (g-$AS_{20}Se_{80}$ and g-$As_{30}Se_{70}$).

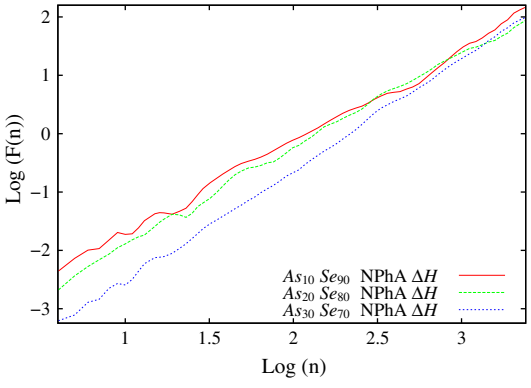

Fig. 5. DFA for NPhA in g-$As_{10}Se_{90}$, g-$As_{20}Se_{80}$ and g-$As_{30}Se_{70}$.

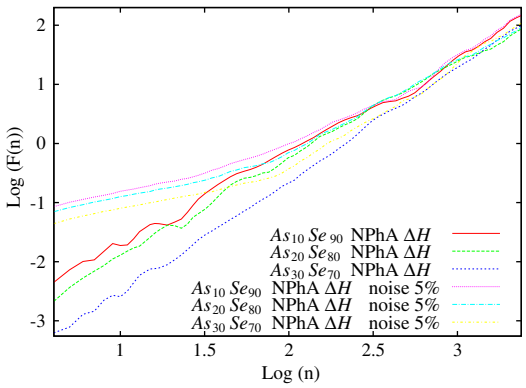

Fig. 6. DFA for NPhA in g-$As_{10}Se_{90}$, g-$As_{20}Se_{80}$, and g-$AS_{30}Se_{70}$ and data with 5% noise added.

Within detrended fluctuation analysis, it was established that starting stages of NPhA in $As_{10}Se_{90}$ and $As_{20}Se_{80}$ have similar characteristics with slope of ~1.57, tending towards ~1.90 with further stages of aging, which is also the slope for g-$As_{30}Se_{70}$. It means that finalizing stage of NPhA is governed by the same type of *As–Se–Se* structural units in g-$As_{10}Se_{90}$, g-$As_{20}Se_{80}$ and g-$As_{30}Se_{70}$ samples. These units are deterministic at all stages of below-T_g structural relaxation in g-$As_{30}Se_{70}$ (from initiating to saturating final stage), while the initiating NPhA in g-$As_{20}Se_{80}$ and g-$As_{30}Se_{70}$ is obviously connected with other type of structural units (preferentially *Se–Se–Se* chains), which can be easily subjected to relaxation.

Thus, the kinetics of enthalpy losses induced by NPhA of Se-rich As–Se glasses can be adequately described via deterministic chaoticity in the reconstructed phase space. The real space pictures of underlying structural transformations responsible for NPhA evolve multiply-repeated cycles of Se atoms twisting within double-well potentials of nearest neighbors followed by atomic shrinkage at larger length scales. This chaotic behavior in NPhA can be treated within potential energy landscape as diversity of transitions between different basins–metabasins towards more thermodynamically equilibrium state, minimizing free energy of the system.

Acknowledgment

The authors would like to thank the editor and referees for their valuable suggestions and comments that helped improve the clarity and the relevance of this manuscript. The authors would like to give thanks to TUBITAK "The Scientific and Technological Research Council of Turkey" under the project number *111T805* and DKNII "The State Agency on Science, Innovations and Informatization of Ukraine" for initiating the international collaboration and providing financial support for this research. This study is also partially supported by the Bogazici University Research Fund.

References

[1] A.V. Kolobov, Photo-induced Metastability in Amorphous Semiconductors, Wiley-VCH, Weinheim, 2003.
[2] K. Tanaka, A. Saitoh, N. Terakado, J. Mater. Sci. Mater. Electron. 20 (2009) 38.
[3] M. Frumar, M. Vlcek, Z. Cernosek, Z. Polak, T. Wagner, J. Non-Cryst. Solids 215 (1997) 213.
[4] K. Shimakawa, A. Kolobov, S.R. Elliott, Adv. Physiol. Educ. 44 (1995) 475.
[5] L.C.E. Struik, Physical Ageing in Amorphous Polymers and Other Materials, Elsevier, New York, 1978.
[6] A. Feltz, Amorphous Inorganic Materials and Glasses, VCH, Weinheim, 1993.
[7] J.M. Saiter, M. Arnoult, J. Grenet, Physica B 355 (2005) 370.
[8] S.H.M. Shieh, W.C. LaCourse, Mater. Chem. Phys. 35 (1993) 160.
[9] R. Golovchak, A. Kozdras, O. Shpotyuk, J. Non-Cryst. Solids 356 (2010) 1149.
[10] K. Shimakawa, N. Nakagawa, T. Itoh, Appl. Phys. Lett. 95 (2009) 051908.
[11] H.D.I. Abarbanel, R. Brown, J.J. Sidorowich, L.Sh. Tsimring, Rev. Mod. Phys. 65 (1993) 1331.
[12] T. Schreiber, Phys. Rep. 308 (1999) 1.
[13] M. Goldstein, J. Chem. Phys. 51 (1969) 3728.

[14] F.H. Stillinger, Science 267 (1995) 1935.
[15] P.G. Debenedetti, F.H. Stillinger, Nature 410 (2001) 259.
[16] S. Sastry, P.G. Debenetti, F.H. Stillinger, Nature 393 (1998) 554.
[17] A. Heuer, J. Phys. Condens. Matter 20 (2008) 373101.
[18] F.H. Stillinger, Phys. Rev. B 41 (1990) 2409.
[19] A. Hacinliyan, Y. Skarlatos, G. Sahin, G. Akin, Chaos, Solitons Fractals 17 (2003) 575.
[20] K. Atak, O.O. Aybar, G. Sahin, A. Hacinliyan, Y. Skarlatos, Cent. Eur. J. Phys. 7 (2009) 568.
[21] R. Golovchak, A. Kovalskiy, A.C. Miller, H. Jain, O. Shpotyuk, Phys. Rev. B 125208–1–7 (2007).
[22] R. Golovchak, H. Jain, O. Shpotyuk, A. Kozdras, A. Saiter, J.M. Saiter, Phys. Rev. B 78 (2008) 014202.
[23] R. Golovchak, A. Kozdras, Cz. Gorecki, O. Shpotyuk, J. Non-Cryst. Solids 352 (2006) 42.
[24] R. Golovchak, Cz Gorecki, A. Kozdras, O. Shpotyuk, Solid State Commun. 137 (2006) 67.
[25] R. Golovchak, A. Kozdras, V. Balitska, O. Shpotyuk, J. Phys. Condens. Matter 24 (2012) 505106.
[26] R. Golovchak, O. Shpotyuk, A. Kozdras, B. Bureau, M. Vlcek, A. Ganjoo, H. Jain, Phil. Mag. 87 (2007) 4323.
[27] R. Golovchak, A. Ingram, A. Kozdras, M. Vlcek, C. Roiland, B. Bureau, O. Shpotyuk, Phil. Mag. 92 (2012) 4182.
[28] B. Bureau, J. Troles, M. LeFloch, F. Smektala, G. Silly, J. Lucas, J. Phys. Condens. Matter 5 (2003) 219.
[29] R. Golovchak, O. Shpotyuk, A. Kozdras, M. Vlcek, B. Bureau, A. Kovalskiy, H. Jain, J. Phys. Condens. Matter 20 (2008) 245101.
[30] J.C. Phillips, J. Non-Cryst. Solids 34 (1979) 153.
[31] M.F. Thorpe, J. Non-Cryst. Solids 57 (1983) 355.
[32] R. Hegger, H. Kantz, T. Schreiber, Chaos 94 (1999) 413.
[33] H. Kantz, Phys. Lett. A 185 (1994) 77.
[34] M.T. Rosenstein, J.J. Collins, C.J.D. Luca, Physica D 73 (1994) 82.
[35] J.P. Eckmann, S.O. Kamphorst, D. Ruelle, Rev. Mod. Phys. 57 (1985) 617.
[36] F. Takens, Dynamical Systems and Turbulence, Lecture Notes in Mathematics, Springer-Verlag, 1981.
[37] T. Sauer, J. Yorke, M. Casdagli, J. Stat. Phys. 65 (1991) 579.
[38] H.G. Schuster, Deterministic Chaos, Wiley-VCH, Wienheim, 2005.
[39] A. Hacinliyan, Y. Skarlatos, G. Sahin, K. Atak, O.O. Aybar, Eur. Phys. J. E 28 (2009) 369.
[40] J.W. Kantelhardt, E.K. Bunde, H.H.A. Rego, S. Havlin, A. Bunde, Physica A 295 (2001) 441.